Assessment of Brain Anatomy with Gradient-Echo Contrasts: A Comparison between Magnitude, Phase, and R2* Imaging with Quantitative Susceptibility Mapping (QSM)

Andreas Deistung[1], Andreas Schäfer[2], Ferdinand Schweser[1], Karsten Sommer[1], Robert Turner[2], and Jürgen Rainer Reichenbach[1]

[1]*Medical Physics Group, Department of Diagnostic and Interventional Radiology I, Jena University Hospital, Jena, Germany,* [2]*Max-Planck-Institute for Human Cognitive and Brain Sciences, Leipzig, Germany*

INTRODUCTION – Accurate assessment of extent and location of anatomical brain structures is essential for many imaging and surgical applications. Superb anatomical contrast has already been demonstrated with T_2^*-weighted magnitude [1] and phase imaging [2, 3] as well as quantitative R_2^* mapping [4] at ultra-high magnetic fields. However, magnitude images are not quantitative, phase images suffer from strong non-local signal contributions and R_2^* images may be affected at locations of steep phase gradients. In contrast, quantitative magnetic susceptibility mapping (QSM) [5], a novel imaging technique that determines tissue magnetic susceptibility from the phase of complex valued gradient echo (GRE) data, provides quantitative and local anatomical contrast. This study compares quantitative susceptibility maps with conventional GRE imaging approaches (magnitude, phase, R_2^*) with respect to anatomic tissue contrast at 7 T and provides quantitative susceptibility and R_2^* values.

MATERIAL AND METHODS – *Data Acquisition:* For susceptibility mapping 3D single-echo GRE data sets (TE/TR/FA/TA=10.5 ms/17ms/8°/16:57min:sec, BW = 140 Hz/px, voxel size=0.4x0.4x0.4mm³) of nine healthy volunteers were acquired on a 7T MR scanner (Magnetom 7T, Siemens Healthcare, Erlangen, Germany) at 3 different orientations of the head with respect to B_0. Additionally, 3D multi-echo GRE imaging (TE_1/TE_2/TE3/TE4=5 ms/12.8 ms/20.6 ms/28.4 ms, TR/FA/BW = 34 ms/8°/160 Hz/px, voxel size of 0.8 × 0.8 × 0.8 mm³) was performed in normal position of the head.

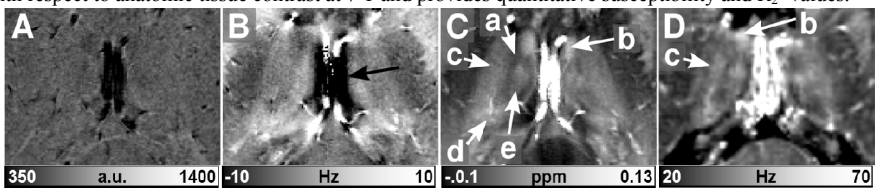

Figure 1: *GRE imaging of the thalamus. Transverse sections of magnitude, frequency, susceptibility, and R_2^* images are shown in (a), (b), (c), and (d), respectively. The susceptibility image clearly exhibits specific contrast within the thalamus enabling discrimination of subthalamic structures, such as a – internal medullary lamina, b – anterior nuclei group, c – ventral lateral nucleus group, d – lateral posterior nucleus, and e – mediodorsal nucleus. In the frequency image (b) such interpretation is impeded by non-local signal contributions, e.g., close-to veins (black arrow).*

Data Processing: Single channel magnitude images were combined using the sum-of-squares method [6], whereas single channel phase images were combined according to [7]. For each subject combined magnitude and phase data sets were non-linearly registered to the dataset in normal position. Phase aliasing was resolved by 3D phase unwrapping [8] and background phase contributions were eliminated with the SHARP technique [5]. Background-corrected phase images were used to compute multi-angle (MA) susceptibility maps as described in [5]. Furthermore, background-corrected phase images were divided by $2\pi \cdot TE$ to yield frequency maps showing the Larmor frequency variation in Hz. The magnitude signal decay of the 3D multi-echo GRE examination was converted to quantitative R_2^* maps according to [9]. For direct comparison the R_2^* images were linearly registered to the susceptibility maps.

Data Analysis: Volumes of interest (VOIs) were manually identified for deep gray matter structures (internal globus pallidus (GPi), external globus pallidus (GPe), putamen (Put), caudate nucleus (CN), subthalamic nucleus (STN), red nucleus (RN), substantia nigra (SN)), homogenous white matter structures (frontal and occipital regions) and corticospinal fluid (CSF). Contrast-to-noise ratio (CNR) was calculated for all image contrasts by calculating the differences in signal intensity between the specific VOI with respect to a VOI in homogeneous white matter in the frontal brain, divided by the noise (standard deviation of the homogeneous white matter VOI). Since noise in MR images scales with MR imaging parameters, e.g., voxel volume and number of averages, the CNR values obtained from susceptibility and R_2^* data were corrected to yield a similar noise level compared to a single GRE data set of the MA study.

	CNR magnitude	CNR frequency	CNR susceptibility	CNR R_2^*	$\Delta\chi$ [ppb]	R_2^* [Hz]
CN	1.02 ± 0.70	3.19 ± 1.58	4.14 ± 1.49	0.43 ± 0.32	25.06 ± 21	42.28 ± 5
GPi	4.00 ± 1.57	1.50 ± 1.18	11.33 ± 2.90	3.01 ± 1.37	98.58 ± 25	81.67 ± 9
GPe	4.13 ± 1.39	1.61 ± 1.32	13.74 ± 3.17	3.23 ± 1.41	123.64 ± 20	85.08 ± 6
Put	0.50 ± 0.33	0.99 ± 0.77	3.58 ± 1.52	0.86 ± 0.5	19.36 ± 19	49.43 ± 7
RN	2.53 ± 0.64	2.05 ± 1.94	8.93 ± 2.12	1.88 ± 0.82	74.84 ± 27	64.92 ± 8
SN	4.37 ± 1.78	2.69 ± 1.93	14.59 ± 3.90	3.03 ± 1.59	132.51 ± 34	81.69 ± 12
STN	3.73 ± 1.40	5.56 ± 3.10	10.43 ± 2.04	2.17 ± 1.04	92.28 ± 38	69.29 ± 9
CSF	1.35 ± 1.45	4.27 ± 1.98	2.11 ± 1.38	2.28 ± 0.85	-	1.22 ± 2

Table 1: *Summary of the VOI analysis. CNR values of selected anatomical regions, averaged over 9 subjects, are presented for magnitude, frequency, susceptibility, and R_2^* images. The cells highlighted in red and yellow reveal the highest and lowest CNR value for each region, respectively. Furthermore, susceptibility differences with respect to CSF (given in parts per billion [ppb]) and R_2^* values (given in Hz) averaged over the 9 subjects are presented in the 2 columns on the left, respectively.*

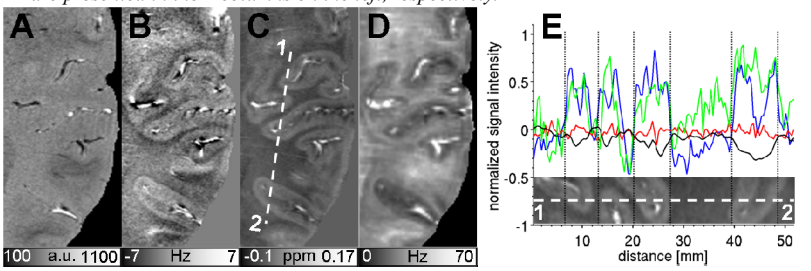

Figure 2: *GRE imaging of cortical grey matter. Magnitude (a), frequency (b), susceptibility (c), and R_2^* (d) images showing the left frontal and parietal lobe are displayed. The dashed line in (c) illustrates the location of the profile line. Normalized signal intensities along this profile for magnitude (red), frequency (green), susceptibility (blue), and R_2^* (black) images are illustrated in (e). The dotted curves in (e) mark regions with high contrast variations between white and cortical grey matter.*

RESULTS & DISCUSSION – A comparison of image contrast within thalamic tissue between magnitude, frequency, susceptibility, and R_2^* images is presented in Figure 1. Magnitude contrast is nearly homogeneous within thalamic tissue and only allows clear identification of the pulvinar (not shown) and venous vessels. Although frequency images provide a heterogeneous signal pattern of thalamic tissue, interpretation is hampered by non-local signal contributions (see black arrow). Susceptibility and R_2^* images, however, provide a very heterogeneous, locally varying pattern of thalamic tissue that clearly enables identification of sub-regions and nuclei of the thalamus. However, the R_2^* images do not provide the same level of contrast and detail as the susceptibility images. The CNR values of different deep grey matter structures for the different images are summarized in Table 1, suggesting that deep gray matter structures are delineated best on susceptibility images. Furthermore, susceptibility differences of selected brain structures with respect to CSF as well as R_2^* values are listed in Table 1. The susceptibility differences are in good agreement with values reported in the literature for 7T [10] and 3T [5, 11]. The R_2^* values (Tab. 1) of the basal ganglia regions agree excellently with literature findings [4]. Susceptibility images provided an excellent and local contrast between white matter and cortical grey matter (Fig. 2) that was superior to the contrast in magnitude, frequency, and R_2^* images (Fig. 2e). Susceptibility maps also revealed sub-structures of the midbrain and basal ganglia that were not observed on corresponding magnitude, frequency, and R_2^* images (not shown). Although QSM based on the MA approach, as presented here, is not applicable in clinical routine, this contribution demonstrates the enormous potential of the susceptibility contrast for structural MRI. QSM may reveal a new contrast for automatic identification of (sub-)structures of the brain.

REFERENCES – [1] Li TQ et al. *NeuroImage*. 2006;32(3):1032-40. [2] Deistung A et al. *Magn Reson Med*. 2008;60(5):1155-68. [3] Duyn JH et al. *Proc Natl Acad Sci U S A*. 2007;104(28):11796-801. [4] Yao B et al. *NeuroImage*. 2009;44(4):1259-66. [5] Schweser F et al. *NeuroImage*. 2011;54(4):2789-807. [6] Roemer PB et al. *Magn Reson Med*. 1990. 16(2):192-225. [7] Hammond KE et al. *NeuroImage*. 2008; 39(4):1682-92. [8] Abdul-Rahman HS et al. *Appl Opt*. 2007;46(26):6623-3. [9] Miller AJ and Joseph PM. *Magn Reson Imaging*. 1993;11(7):1051-6. [10] Wharton S and Bowtell R. *NeuroImage*. 2010;53(2), 515-525. [11] Liu T et al. *Magn Reson Med*. 2011;66(3), 777-83.